MASSACHUSETTS INSTITUTE OF TECHNOLOGY
ARTIFICIAL INTELLIGENCE LABORATORY

A.I.Memo No. 1032 October, 1988

Real-Time Part Position Sensing

Steven J. Gordon
Warren P. Seering

Abstract: A light stripe vision system is used to measure the location of polyhedral features of parts from a single frame of video camera output. Issues such as accuracy in locating the line segments of intersection in the image and combining redundant information from multiple measurements and multiple sources are addressed. In 2.5 seconds, a prototype sensor was capable of locating a two inch cube to an accuracy (one standard deviation) of .002 inches (.055 mm) in translation and .1 degrees (.0015 radians) in rotation. When integrated with a manipulator, the system was capable of performing high precision assembly tasks.

Acknowledgements: The research described in this paper was performed at the Massachusetts Institute of Technology Artificial Intelligence Laboratory. The laboratory's research is funded in part by the Defense Advanced Research Projects Agency of the U.S. Department of Defense under ONR contract N00014-85-K-0124, Office of Naval Research University Research Initiative Program under ONR contract N00014-86-K-0685 and IBM Corporation.

From **IEEE Transanctions on Pattern Analysis and Machine Intelligence**, May, 1988, Vol. 10 No. 3

1 Introduction

Fast and accurate location of objects is important in many automated industrial tasks involving inspection, assembly and machining. Such a measurement capability can change the way certain tasks are currently performed, for instance, force controlled motion and precise part fixturing are unnecessary if an assembly system can align mating surfaces of parts.

An interest in automating mechanical assembly tasks prompted a study of sensing systems which provide computers with information about the position of parts. The most critical sensor design requirements for a position-sensor-based assembly system are high speed and accurate operation; thus, many of the object ranging systems in the literature [3,8,20,21,30,34] cannot be used.

The system described in this paper operates in a relatively highly constrained industrial environment. We assume that the *a priori* position of a part is known approximately; that is, the expected location of the part is available to the sensor before it makes a measurement. With this assumption, fairly sparse data may be used to obtain a relatively precise measurement. A conceptually similar approach was taken by Benton and Waters [5] and Rutkowski et al. [29] who fit a model to light stripe data. Their approach depended upon an iterative technique and was somewhat slower and less accurate than the technique discussed here, however, it could locate a larger variety of part features.

2 Sensing Method

A system capable of making measurements in six degrees of freedom is required for the part position sensing function. In addition, a flexible (capable of measuring many different parts), high speed, high accuracy, and low cost system is desirable. Jarvis [24] presents an overview of a number of three-dimensional ranging systems. The light stripe ranging technique was selected because it best fits the sensing system requirements.

The light plane of a light stripe system is projected across one or more features (such as a corner of a polyhedron or an end of a truncated circular cylinder) of a part, Figure 1. Data from an image taken by a video camera positioned at some disparate angle with respect to the light plane is processed to locate the feature.

Triangulation is used to obtain three-dimensional data from the two-dimensional sensing element data, Figure 2. A common light source for light stripe systems is a laser beam which has been passed through a cylindrical lens. The lens diverges the beam in a direction perpendicular to the lens' cylindrical axis.

The light plane is the sole functional illumination source in the scene as viewed by the camera. An isomorphism exists between all points in the image and points lying in the light plane in three-space. In order to determine the transformation

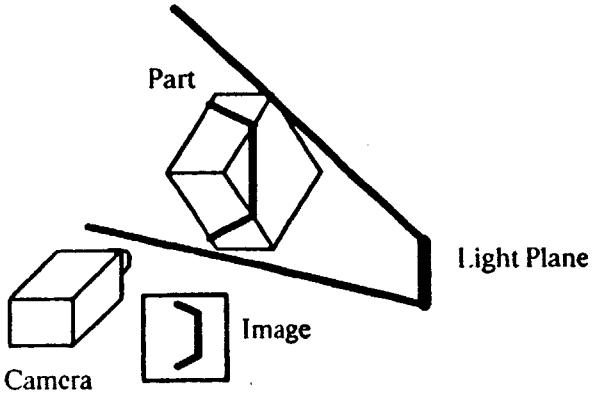

Figure 1: Three line segments generated by the intersection of a plane of light and the surfaces of a polyhedral feature may be sensed by a video camera and used to locate a part.

from the two-dimensional image coordinates to accurate three-dimensional space coordinates, the system must be precisely calibrated. During the calibration, the values of three parameters must be determined which locate the light plane with respect to a coordinate frame defined by the camera image plane. A disparity angle, θ_{LP}, a tilt angle, ϕ_{LP}, and an offset, y_{LP}, are the parameters used for defining the light plane location (these are not unique).

Discussion in this paper is limited to objects whose surfaces are planar (actually only those surfaces being sensed need be planar); thus, the intersection curves between the light plane and part surfaces are line segments.

2.1 Inverse Projection of Image Points

The coordinates of points in space lying in the light plane may be derived as a function of the image plane coordinates and the light plane and camera calibration parameters. Some authors have used a matrix description for the geometry of a light stripe system [2,26]. Separate equations are maintained here. The transformation of a point on an object, (x, y, z), to image plane coordinates, (y_I, z_I), is described by the perspective projection [35]

$$y_I = -\frac{y f_0}{x}$$
$$z_I = -\frac{z f_0}{x} \tag{1}$$

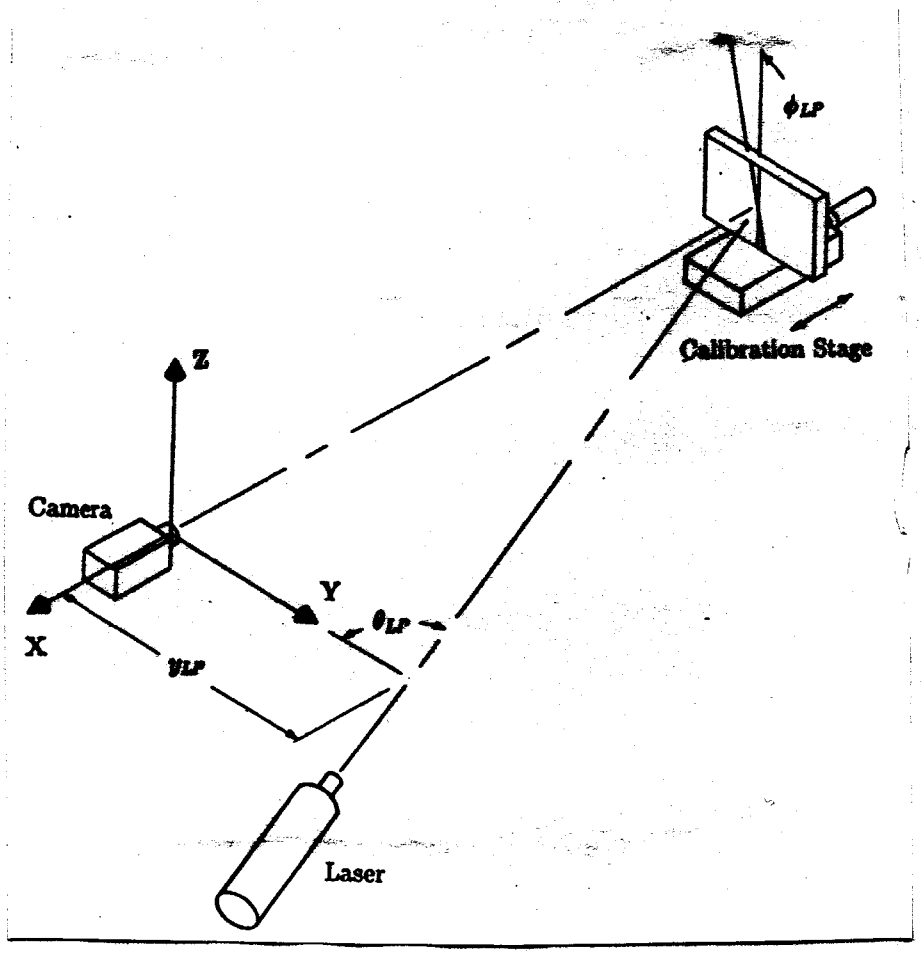

Figure 2: Light stripe [illegible]

We may obtain the x coordinate in terms of the y and z coordinates using the light plane constraint. From Figure 2

$$x = x_0 + \tan\theta_{LP}\,(y + z\tan\phi_{LP}) \tag{2}$$

where x_0 is the position along the optical axis where the light plane crosses,

$$x_0 = -y_{LP}\tan\theta_{LP}.$$

In general $x_0 < 0$. Combining (1), and (2), we obtain

$$x = \frac{x_0}{1+\tan\theta_{LP}(\tan\phi_{LP}\frac{z_I}{f_0}+\frac{y_I}{f_0})} \tag{3}$$

$$y = -\frac{\frac{y_I}{f_0}x_0}{1+\tan\theta_{LP}(\tan\phi_{LP}\frac{z_I}{f_0}+\frac{y_I}{f_0})} \tag{4}$$

$$z = -\frac{\frac{z_I}{f_0}x_0}{1+\tan\theta_{LP}(\tan\phi_{LP}\frac{z_I}{f_0}+\frac{y_I}{f_0})}. \tag{5}$$

These equations describe the position of a point in space (x, y, z) as a function of the coordinates of the corresponding point in the image plane (y_I, z_I).

2.2 Calculation of Three-Dimensional Vectors from the Light Stripe Image

The measurements obtained from the image of the intersection of a light plane and a polyhedral feature is a set of line parameters, $[m_{I,i}, b_{I,i}]$, which are defined by the equation of the line (refer to Figure 3)

$$y_I = m_{I,i}z_I + b_{I,i}. \tag{6}$$

Using (3), (4), (5), and (6) we may obtain expressions for the vectors along the light stripes in real space, $\vec{l_i}$, and vectors from the origin to the intersection of the light stripes and the $z = 0$ plane, $\vec{b_i}$,

$$\vec{l_i} = \begin{Bmatrix} (m_i + \tan\phi_{LP})\tan\theta_{LP} \\ m_i \\ 1 \end{Bmatrix} \tag{7}$$

and

$$\vec{b_i} = \begin{Bmatrix} \frac{x_0}{1+\frac{b_{I,i}}{f_0}\tan\theta_{LP}} \\ -\frac{x_0\frac{b_{I,i}}{f_0}}{1+\frac{b_{I,i}}{f_0}\tan\theta_{LP}} \\ 0 \end{Bmatrix} \tag{8}$$

where

$$m_i = \frac{m_{I,i} - \frac{b_{I,i}}{f_0}\tan\phi_{LP}\tan\theta_{LP}}{1+\frac{b_{I,i}}{f_0}\tan\theta_{LP}}. \tag{9}$$

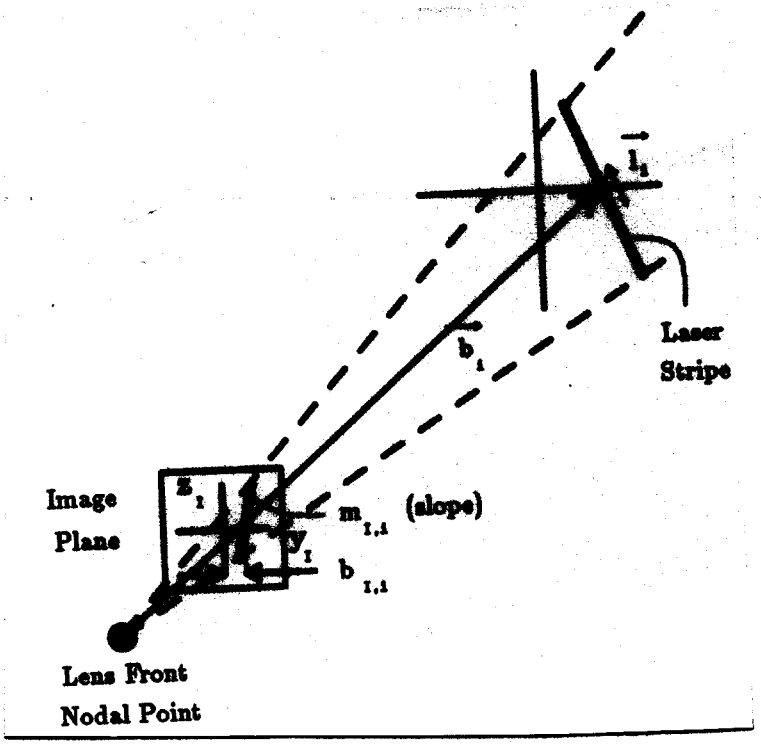

Figure 3: Parameters for a line in the image plane and vectors specifying the light stripe.

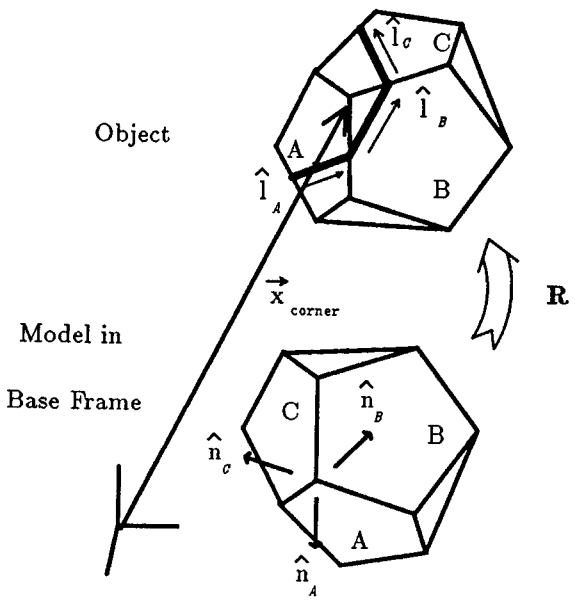

Figure 4: Light plane intersecting a polyhedral feature and a corresponding model of the feature.

3 Polyhedral Feature Localization

Most of the light stripe systems in the literature require scanning a complete scene and processing a number of video frames. With the light plane positioned at a certain orientation with respect to a polyhedron, three or more line segments comprise the curve of intersection and only a single frame is necessary to locate the part given its approximate *a priori* position. The following geometric conditions are sufficient for three light plane intersection lines to locate a part [32]

- Pairs of lines must not be parallel.
- Pairs of faces in which lines lie must not be parallel.
- The common normal of any pair of lines must not be parallel to the line of intersection of any two faces in which the lines lie.

3.1 Locating General Polyhedral Features

The position of a polyhedral feature of an object is referenced relative to a model of the feature in a base coordinate system, Figure 4. The orientation of the feature may be determined by the slopes of three line segments in the image. The displacement may be determined from the results of the orientation calculation and

the intercepts of the three lines; thus, the orientation calculation may be decoupled from the displacement calculation.

3.1.1 Determining the Orientation

We wish to find the rotation between the model and the object. Assume that the three normal vectors for faces A, B, and C of the model in Figure 4 are $\hat{n}_A$, $\hat{n}_B$, and $\hat{n}_C$ respectively. The normal vectors of the object are unknown, but vectors along the intersection line segments on the object are known from the sensed data. Assuming that the correspondence between faces is known (approximate *a priori* position), the unit vectors along the intersection line segments for faces A, B, and C are $\hat{l}_A$, $\hat{l}_B$, and $\hat{l}_C$ respectively. The rotation matrix $\mathbf{R}$ from the model to the object is found using quaternion notation [23,28,31]. We denote a quaternion by the bold face letter, $\mathbf{q}$. Every quaternion has a corresponding four vector, $\vec{q}$, whose components are the four elements of the quaternion. A quaternion with a zero scalar element represents a three vector; thus a quaternion multiplied by a vector is defined. A rigid rotation of a vector $\vec{v}$ is

$$\mathbf{q}\vec{v}\mathbf{q}^*$$

where $\mathbf{q}$ is a unit quaternion and $\mathbf{q}^*$ is the quaternion complement of $\mathbf{q}$.

If the proper rotation is found, the line vectors, $\hat{l}_i$, will be perpendicular to the rotated model normal vectors, $\mathbf{q}\hat{n}_i\mathbf{q}^*$; that is, the dot product will be zero

$$\hat{l}_i \cdot \mathbf{q}\hat{n}_i\mathbf{q}^* = 0, \quad i = A, B, C. \tag{10}$$

Each of these equations are quadratic in components of $\mathbf{q}$. Rewriting this in matrix form

$$\begin{aligned} \vec{q}^T \mathbf{A}_i \vec{q} &= 0, \quad i = A, B, C, \\ |\vec{q}| &= 1 \end{aligned} \tag{11}$$

which is a coupled set of four quadratic equations. Each of the three $\mathbf{A}_i$ matrices (4×4) have elements of quadratic polynomials in components of l_j and n_k (j and k take on values of A, B or C). The components of $\vec{q}$ may be determined using any of a number of numerical methods. The rotation matrix, $\mathbf{R}$, may be calculated from the components of $\mathbf{q}$ [31]

$$\mathbf{R} = \begin{bmatrix} q_0^2 + q_1^2 - q_2^2 - q_3^2 & 2(-q_0q_3 + q_1q_2) & 2(q_0q_2 + q_1q_3) \\ 2(q_0q_3 + q_1q_2) & q_0^2 - q_1^2 + q_2^2 - q_3^2 & 2(-q_0q_1 + q_2q_3) \\ 2(-q_0q_2 + q_1q_3) & 2(q_0q_1 + q_2q_3) & q_0^2 - q_1^2 - q_2^2 + q_3^2 \end{bmatrix}.$$

An alternate approach to locating the general polyhedral feature is to use an iterative method such as the one in [5,29]. The assumed *a priori* location of the feature provides a good initial guess and improves solution convergence.

3.1.2 Determining the Displacement

Once the rotation from the model to the object is known, the normal vectors of the object, $\hat{n}_{obj,i}$, may be calculated

$$\hat{n}_{obj,i} = \mathbf{R}\hat{n}_i, \quad i = A, B, C. \tag{12}$$

Unless an intersection line is parallel to the $z = 0$ plane, we may define the intercept vector, $\vec{b}_i$, which lies in the $z = 0$ plane from the origin to the i^{th} intersection line. The equation of the plane which lies on the i^{th} face is [15]

$$(\vec{x} - \vec{b}_i) \cdot \hat{n}_{obj,i} = 0 \tag{13}$$

where $\vec{x} = [x\ y\ z]^T$ is the location of a point in space. Solving these three equations simultaneously for the planes on faces A, B, and C, we obtain the location of the corner

$$\vec{x}_{corner} = \frac{p_A(\hat{n}_{obj,B} \times \hat{n}_{obj,C}) + p_B(\hat{n}_{obj,C} \times \hat{n}_{obj,A}) + p_C(\hat{n}_{obj,A} \times \hat{n}_{obj,B})}{\hat{n}_{obj,A} \cdot (\hat{n}_{obj,B} \times \hat{n}_{obj,C})} \tag{14}$$

where $\times$ denotes the vector product and p_i is the perpendicular distance from the origin to the i^{th} plane

$$\begin{aligned} p_A &= (b_A \cdot \hat{n}_{obj,A}) \\ p_B &= (b_B \cdot \hat{n}_{obj,B}) \\ p_C &= (b_C \cdot \hat{n}_{obj,C}). \end{aligned} \tag{15}$$

3.2 Locating Right Corner Features

The solution for the rotation of the right polyhedral corner feature may be solved in closed form (in contrast to using a numerical technique for general polyhedra). We define a right corner feature as the intersection of three half spaces (see Figure 5) whose bounding planes are mutually orthogonal. A right-hand coordinate system, $\mathcal{F}_F$, with axes $\hat{x}_F$, $\hat{y}_F$, $\hat{z}_F$ perpendicular to the bounding planes of the half spaces and origin located at the point of intersection of the bounding planes defines the position of the feature in six degrees of freedom. We wish to determine the orientation and position of this feature reference frame with respect to the world frame, $\mathcal{F}_W$, located at the camera image plane.

3.2.1 Determining the Orientation

The orientation of the feature reference frame, $\mathcal{F}_F$, with respect to the world reference frame, $\mathcal{F}_W$, is determined by locating an intermediate reference frame

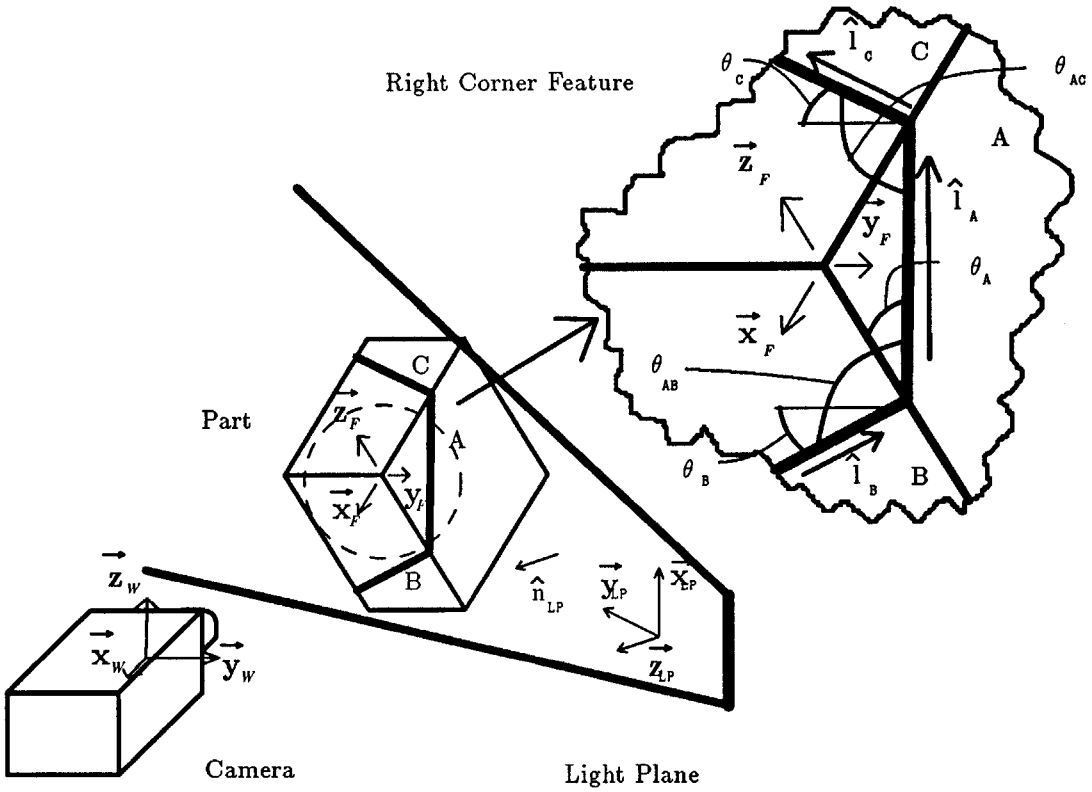

Figure 5: A right corner feature and reference frames used to determine its orientation.

.

associated with the laser plane, $\mathcal{F}_{LP}$. For the present analysis, we assume that the light plane has no width (two-dimensional). We also assume that three line segments (no width) are generated when the light plane intersects the feature. The orientation of the three line segments are defined by the three vectors $\hat{l}_A$, $\hat{l}_B$, and $\hat{l}_C$ as shown in Figure 5.

We assume the ranging sensor has been accurately calibrated and the unit vector normal to the light plane, $\hat{n}_{LP}$, is known. The intermediate coordinate system, $\mathcal{F}_{LP}$, has axes $\hat{x}_{LP}$ in direction of one of the lines of intersection ($\hat{l}_A$), $\hat{z}_{LP}$ in direction $\hat{n}_{LP}$, and $\hat{y}_{LP}$ in direction $\hat{n}_{LP} \times \hat{l}_A$.

The rotational transformation (in matrix form) from $\mathcal{F}_W$ to $\mathcal{F}_{LP}$ is

$$\mathbf{R}_{W,LP} = \left[\hat{l}_A, \ \hat{n}_{LP} \times \hat{l}_A, \ \hat{n}_{LP}\right] \tag{16}$$

$\mathcal{F}_{LP}$ may be located with respect to $\mathcal{F}_F$ by realizing that the cross product of any two of the three vectors $\hat{l}_A$, $\hat{l}_B$, or $\hat{l}_C$ is normal to the light plane (in the direction of $\hat{z}_{LP}$) and $\hat{l}_A$ lies on the $\hat{y}_F, \hat{z}_F$ plane. The transformation from $\mathcal{F}_W$ to $\mathcal{F}_{LP}$ is[1]

$$\begin{aligned} \mathbf{R}_{F,LP} &= \left[{}^F\hat{l}_A, \ ({}^F\hat{l}_B \times {}^F\hat{l}_A) \times {}^F\hat{l}_A, \ {}^F\hat{l}_B \times {}^F\hat{l}_A\right] \\ &= \begin{bmatrix} 0 & \frac{\sin\theta_B}{\sqrt{\cos^2\theta_A \sin^2\theta_B + \sin^2\theta_A}} & \frac{\sin\theta_A \cos\theta_B}{\sqrt{\cos^2\theta_A \sin^2\theta_B + \sin^2\theta_A}} \\ -\cos\theta_A & \frac{\sin^2\theta_A \cos\theta_B}{\sqrt{\cos^2\theta_A \sin^2\theta_B + \sin^2\theta_A}} & \frac{-\sin\theta_B \sin\theta_A}{\sqrt{\cos^2\theta_A \sin^2\theta_B + \sin^2\theta_A}} \\ -\sin\theta_A & \frac{-\cos\theta_B \cos\theta_B \sin\theta_A}{\sqrt{\cos^2\theta_A \sin^2\theta_B + \sin^2\theta_A}} & \frac{\sin\theta_B \cos\theta_A}{\sqrt{\cos^2\theta_A \sin^2\theta_B + \sin^2\theta_A}} \end{bmatrix} \end{aligned} \tag{17}$$

where θ_A is the angle between $\hat{l}_A$ and $\hat{z}_F$, and θ_B is the angle between $\hat{l}_B$ and y_F. The angles θ_A and θ_B may be calculated from the angle between $\hat{l}_A$ and $\hat{l}_C$ (θ_{AC}) and the angle between $\hat{l}_A$ and $\hat{l}_B$ (θ_{AB}) (these angles are both easily obtainable from the processed image)

$$\begin{aligned} \theta_A &= \arctan\sqrt{-\frac{\tan\theta_{AB}}{\tan\theta_{AC}}} \\ \theta_B &= \arccos\frac{\cos\theta_{AB}}{\cos\theta_A}. \end{aligned}$$

Multiple values of the rotation matrix, $\mathbf{R}_{F,LP}$, which correspond to different light stripe image interpretations result from these equations. The proper rotation matrix is the one closest to the expected nominal rotation matrix. The orientation of the feature reference frame, $\mathcal{F}_F$, with respect to the world coordinate frame, $\mathcal{F}_W$, is:

$$\mathbf{R}_{W,F} = \mathbf{R}_{W,LP}\mathbf{R}_{F,LP}^{-1} \tag{18}$$

[1]The left superscripts ${}^F\hat{l}$ denotes that the vector is expressed with respect to the $\mathcal{F}_F$ reference frame.

Variable	Description
$\mathcal{L}$	Line target
$\mathcal{L}_{image}$	Image of $\mathcal{L}$ in the camera's image plane
N	Number of illuminated pixels.
$(\bar{x}_i, \bar{y}_i)$	Coordinates of the center of the i^{th} illuminated pixel
(x_i, y_i)	Coordinates (probabilistic) of points lying on $\mathcal{L}_{image}$
δy_i	Probabilistic distance in the y direction from the center of the i^{th} illuminated pixel to $\mathcal{L}_{image}$
θ	Orientation angle of $\mathcal{L}$ measured counterclockwise from the x axis
y_0	y axis intercept of $\mathcal{L}$
$\hat{\theta}$, $\hat{y_0}$	Least squares estimators for θ and y_0
$\bar{\theta}$, $\bar{y_0}$	Estimators for θ and y_0 from discrete data $(\bar{x}_i, \bar{y}_i)$
$\Delta\bar{\theta}$, $\Delta\bar{y_0}$	Difference between estimated line parameters $(\bar{\theta}, \bar{y_0})$ and actual parameters (θ, y_0)
L_{pixel}	Length of each square pixel
σ_y^2	Variance of δy_i for all $i = 1, \ldots N$
x_{cm}	Distance from the center of $\mathcal{L}_{image}$ to the y axis measured parallel to the x axis

Table 1: Nomenclature for line parameter error analysis.

3.2.2 Determining the Displacement

Once the rotation is known, the displacement of the corner from the base coordinate system is given by 14.

4 Locating Straight Line Features in Quantized Images

Determining the accuracy of measurements of polyhedral features is studied by addressing the more fundamental problem of determining the accuracy of fitting two-dimensional line segment parameters. The precision of a least squares technique in determining the orientation and position of thin line segments in the presence of quantization noise is investigated. The probabilistic technique used in this study is similar to the one reported by Hill [22].

4.1 Errors in Fitting Linear Parameters to Discretized Data

Data generated by straight-line features appear as discrete points of various intensities located within some width of a central axis in the image plane of a discrete array sensor. These points can be processed to find the best fit line through them using a least squares technique [1,4]. This section explores the accuracy with which straight line features may be found. The variables used in the subsequent analysis are listed in Table 1.

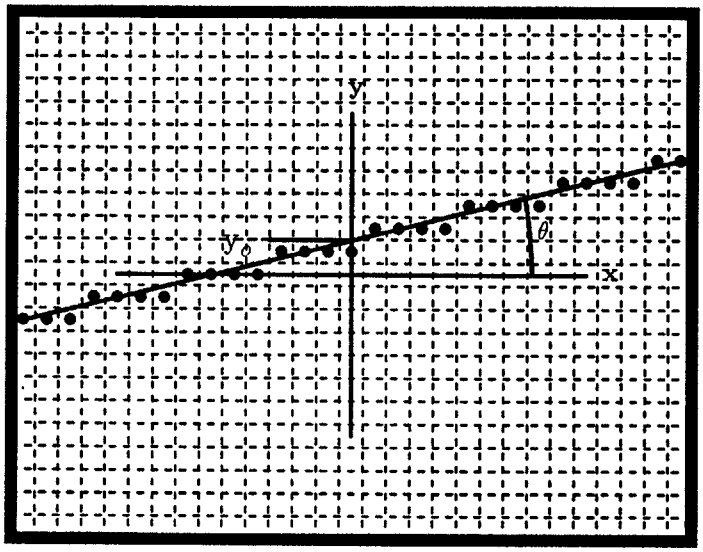

Figure 6: Parameters for the image of a line (infinitely thin).

4.1.1 Theoretical Errors from Linear Least Squares Approximations

For the following analysis it is assumed that an image is generated from a single line (infinitely thin), $\mathcal{L}$, which lies in a plane parallel to the image plane. The line is located at orientation θ from the horizontal (x) axis and passes over the y axis at intercept y_0. For simplification, the projection of $\mathcal{L}$ into the image plane produces an image, $\mathcal{L}_{image}$ identical to $\mathcal{L}$ (that is, the angle and intercept remain θ and y_0 respectively – see Figure 6). A typical output from a CCD (charge coupled device) video camera (the only type being considered here) is an analog signal constructed from a number of intensity readings from discrete pixels in a rectangular grid. For this analysis, we assume that the image has been thresholded and transformed into a binary array of square elements with length L_{pixel}.

For geometric reasons, when $\theta \in [\frac{\pi}{4}, \frac{3}{4}\pi]$, one pixel per row is illuminated and when $\theta \in [-\frac{\pi}{4}, \frac{\pi}{4}]$, only one pixel for every column is illuminated. We define an illuminated pixel as the one in a particular row (or column) whose border circumscribes the longest segment of $\mathcal{L}_{image}$. Although this definition loses some positional information from the array, it simplifies the subsequent analysis. Later in this section corrections from grey level information are suggested which preserve more of the available positional information.

The sensor data used for curve fitting is a list of pixel center coordinates for the illuminated elements $(\bar{x}_i, \bar{y}_i)$ $i = 1, \ldots N$. A "best fit" orientation and intercept ($\widehat{\theta}$ and $\widehat{y_0}$ respectively) may be found in the least squares sense by minimizing the sum of the squares of the distances from the best fit line to data points $(\bar{x}_i, \bar{y}_i)$ with

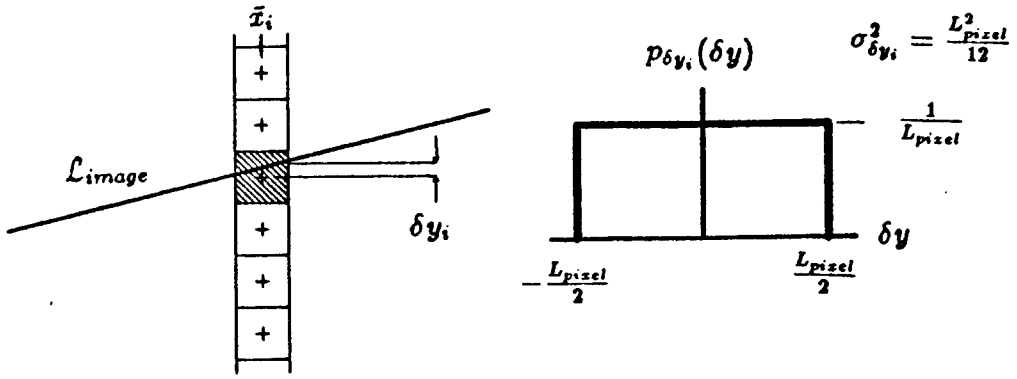

a. b.

Figure 7: Probabilistic location of points on a line. a. Intersection of a column of pixels with a line in the range $\theta \in [-\frac{\pi}{4}, \frac{\pi}{4}]$. b. Probability density function for the location of the y coordinate of $\mathcal{L}_{image}$ measured from the center of the illuminated pixel.

distance measured one of three ways:

A: *Minimize distances parallel to the y axis.*

B: *Minimize distances parallel to the x axis.*

C: *Minimize distances perpendicular to the line.*

Each of these gives a slightly different result for $\hat{\theta}$ and $\widehat{y_0}$ and the best choice is not immediately apparent.

Selection of the most appropriate metric to minimize depends upon the gross orientation of $\mathcal{L}$. As a result of our definition of an illuminated pixel, (one pixel for every y coordinate is illuminated when $\theta \in [\frac{\pi}{4}, \frac{3}{4}\pi]$, and one pixel for every x coordinate is illuminated when $\theta \in [-\frac{\pi}{4}, \frac{\pi}{4}]$), we can choose an x coordinate in the first case which is deterministic ($\bar{x}_i$ will always correspond to a point on the line within that pixel – see Figure 7a), and a y coordinate in the second case which is deterministic. With these choices of coordinates, we should minimize errors in probabilistic coordinates y_i in the first case (metric A) and x_i in the second case (metric B).

In the subsequent analysis θ is assumed to lie in the interval $[-\frac{\pi}{4}, \frac{\pi}{4}]$. The least squares estimates for orientation $\hat{\theta}$ and intercept $\widehat{y_0}$ are found by minimizing errors parallel to the y axis [1,4]

$$\hat{\theta} = \arctan \frac{\sum_{i=1}^{N} y_i x_i - \frac{\sum_{i=1}^{N} x_i \sum_{i=1}^{N} y_i}{N}}{\sum_{i=1}^{N} x_i^2 - \frac{(\sum_{i=1}^{N} x_i)^2}{N}} \tag{19}$$

$$\widehat{y_0} = \frac{\sum_{i=1}^{N} y_i - \tan\hat{\theta} \sum_{i=1}^{N} x_i}{N} \tag{20}$$

where (x_i, y_i) are the coordinates of points lying on $\mathcal{L}_{image}$. If (x_i, y_i) were known precisely, the least squares estimates would be identical to the actual line parameters; however, in the interval $\theta \in [-\frac{\pi}{4}, \frac{\pi}{4}]$, only precise x_i values are available.

We are considering the case where x_i is deterministic and y_i is probabilistic and we desire a metric for the confidence of the estimated line parameters $\hat{\theta}$ and $\widehat{y_0}$ calculated from the measurements $(\bar{x}_i, \bar{y}_i)$. We shall derive the variance of $\hat{\theta}$ and $\widehat{y_0}$ ($\sigma^2_{\hat{\theta}}$ and $\sigma^2_{\widehat{y_0}}$ respectively) as a function of all $(\bar{x}_i, \bar{y}_i)$'s and the variance of y_i ($\sigma^2_{y_i}$).

Each random variable y_i may be written as

$$y_i = \bar{y}_i + \delta y_i \tag{21}$$

where $\bar{y}_i$ is deterministic and δy_i is a random variable with zero mean. At first it might appear that the δy_i's are highly correlated since they all lie on the same line; however, some authors [22,27] have suggested that independence between δy_i's is a good assumption for certain cases. In the case of the straight line, the degree of correlation depends upon the orientation of the line. At some orientations, the values of δy_i may change in an unrelated fashion (slightly correlated) while at other orientations, the values of δy_i may exhibit a periodic pattern (highly correlated). We make the initial assumption that the δy_i's are independent and a supposition that this might not be valid for lines at certain orientations.

If the maximum absolute value of the δy_i's are small, (19) and (20) can be linearized about the points $(\bar{x}_i, \bar{y}_i)$ by taking the Taylor series expansion, and keeping the first two terms

$$\hat{\theta} \approx \bar{\hat{\theta}} + \sum_{i=1}^{N} \left(\frac{\partial \hat{\theta}}{\partial y_i} \right)_{(\bar{x}_i, \bar{y}_i)} \delta y_i \tag{22}$$

$$\widehat{y_0} \approx \bar{\widehat{y_0}} + \sum_{i=1}^{N} \left(\frac{\partial \widehat{y_0}}{\partial y_i} \right)_{(\bar{x}_i, \bar{y}_i)} \delta y_i \tag{23}$$

where $\left(\frac{\partial}{\partial y_i}\right)_{(\bar{x}_i, \bar{y}_i)}$ is the partial derivative with respect to y_i evaluated at $(\bar{x}_i, \bar{y}_i)$ and

$$\bar{\hat{\theta}} = \arctan \frac{\sum_{i=1}^{N} \bar{y}_i \bar{x}_i - \frac{\sum_{i=1}^{N} \bar{x}_i \sum_{i=1}^{N} \bar{y}_i}{N}}{\sum_{i=1}^{N} \bar{x}_i^2 - \frac{(\sum_{i=1}^{N} \bar{x}_i)^2}{N}} \tag{24}$$

$$\bar{\widehat{y_0}} = \frac{\sum_{i=1}^{N} \bar{y}_i - \tan \bar{\hat{\theta}} \sum_{i=1}^{N} \bar{x}_i}{N}. \tag{25}$$

For all δy_i independent of one another [10]

$$\sigma^2_{\hat{\theta}} \approx \sum_{i=1}^{N} \left(\frac{\partial \hat{\theta}}{\partial y_i} \right)^2_{(\bar{x}_i, \bar{y}_i)} \sigma^2_{\delta y_i} \tag{26}$$

$$\sigma^2_{\widehat{y_0}} \approx \sum_{i=1}^{N} \left(\frac{\partial \widehat{y_0}}{\partial y_i} \right)^2_{(\bar{x}_i, \bar{y}_i)} \sigma^2_{\delta y_i}. \tag{27}$$

Substituting (19) and (20) into (26) and (27) respectively then making the assumption that all δy_i have the same variance σ_y^2, and setting x_i to $\bar{x}_i$, we obtain

$$\sigma^2_{\widehat{\theta}} \approx \frac{1}{(1+\bar{m}^2)^2} \frac{\sigma_y^2}{\left(\sum_{i=1}^{N} \bar{x}_i^2 - \frac{(\sum_{i=1}^{N} \bar{x}_i)^2}{N} \right)} \tag{28}$$

$$\sigma^2_{\widehat{y_0}} \approx \frac{1}{N} \left(1 + \frac{\frac{(\sum_{i=1}^{N} \bar{x}_i)^2}{N}}{\sum_{i=1}^{N} \bar{x}_i^2 - \frac{(\sum_{i=1}^{N} \bar{x}_i)^2}{N}} \right) \sigma_y^2 \tag{29}$$

where

$$\bar{m} = \frac{\sum_{i=1}^{N} \bar{y}_i \bar{x}_i - \frac{\sum_{i=1}^{N} \bar{x}_i \sum_{i=1}^{N} \bar{y}_i}{N}}{\sum_{i=1}^{N} \bar{x}_i^2 - \frac{(\sum_{i=1}^{N} \bar{x}_i)^2}{N}}.$$

Equations (28) and (29) give the variances of the fitted line parameters as a function of the data points $(\bar{x}_i, \bar{y}_i)$ and the variance of the location of the y coordinate of the line in any column containing an illuminated pixel (similar results are obtained in [4]).

If columns $\bar{y}_i$ have an illuminated pixel for all $i = 1, \ldots N$ then the expressions for the variance of $\widehat{\theta}$ and $\widehat{y_0}$ become

$$\sigma^2_{\widehat{\theta}} \approx \frac{1}{(1+\bar{m}^2)^2} \frac{12\sigma_y^2}{N^3 - N} \tag{30}$$

$$\sigma^2_{\widehat{y_0}} \approx \left(\frac{1}{N} + \frac{12 x_{cm}^2}{N^3 - N} \right) \sigma_y^2 \tag{31}$$

where $x_{cm} = \frac{\sum_{i=1}^{N} \bar{x}_i}{N}$ is the calculated center of the line segment in the x direction.

These results describe the accuracy with which a line may be found from a least squares technique as a function of the approximate slope $(\bar{m})$, the orthographic projection of the length of the line (in pixels) onto the x axis (N), the center of the line in the x direction (x_{cm}), and the variance of the location of the y coordinate for any one column of the image (σ_y^2). $\sigma^2_{\widehat{\theta}}$ does not depend on the position of the line segment in the pixel grid, while $\sigma^2_{\widehat{y_0}}$ depends on the distance of the center of the line segment from the y axis. For a line (zero width), the probability density function for mutually independent δy_i is a uniform distribution one pixel in width with a $\sigma^2_{\delta y_i} = \sigma_y^2 = \frac{L^2_{pixel}}{12}$ (see Figure 7b). The standard deviations $\sigma_{\widehat{\theta}}$ and $\sigma_{\widehat{y_0}}$ are plotted in Figure 8 as a function of the number of points N for a line positioned near $\theta = 0$ and with $x_{cm} = \frac{N}{2}$.

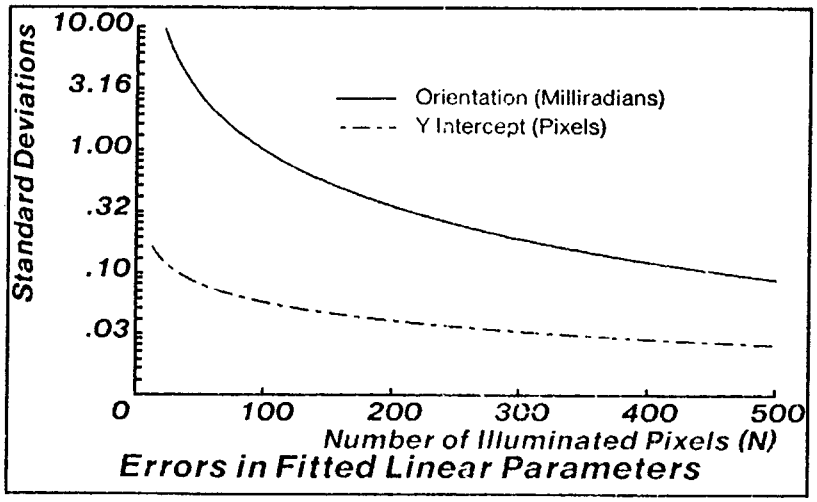

Figure 8: Standard deviations for orientation and y intercept estimates as a function of the number of illuminated pixels.

The above analysis is valid for a grey scale images of finite width lines as well as binary images of thin lines. If $\bar{y}_i$ is permitted to take on subpixel values, and grey scale levels are used in an intensity weighted calculation for the center of the line, $\bar{y}_i$ becomes a better estimate of the actual value y_i (σ_y^2 would be smaller – see [17]). The reduction in σ_y^2 is a function of the width of the line and the resolution (in intensity measurements) of the camera.

In support of the theoretical analysis, computer simulations and experimental tests were performed. In both studies, sample statistics from 30 trials were calculated and used as a basis for comparisons. Figure 9 shows the results of the study with statistics generated in each of eighteen equally spaced orientations from zero to forty-five degrees. The sample standard deviations for each set of thirty trials (each trial is at a different random orientation within a 2.5 degree range) with a line 128 pixels long are plotted for each interval along with the theoretical result, (30). A plot of the accuracy of fitted parameters of lines from 45 to 90 degrees from metric B would appear as the mirror-image of Figure 9 about the 45 degree position. Singularities in $\Delta\hat{\theta}$ occur at slopes near 0, $\frac{1}{4}$, $\frac{1}{3}$, $\frac{1}{2}$, $\frac{3}{4}$, and 1 (shown in figure). In these areas, measurements of the location and orientation of $\mathcal{L}_{image}$ are not as accurate because there is more space for $\mathcal{L}$ to translate and rotate before pixels are caused to change state. (see Figure 10). The theoretical result does not predict these singularities because the mutual independence assumption is not valid there. The simulation and experimental sample standard deviations at all orientations are, however, theoretically bounded by an analysis assuming perfect correlation [18].

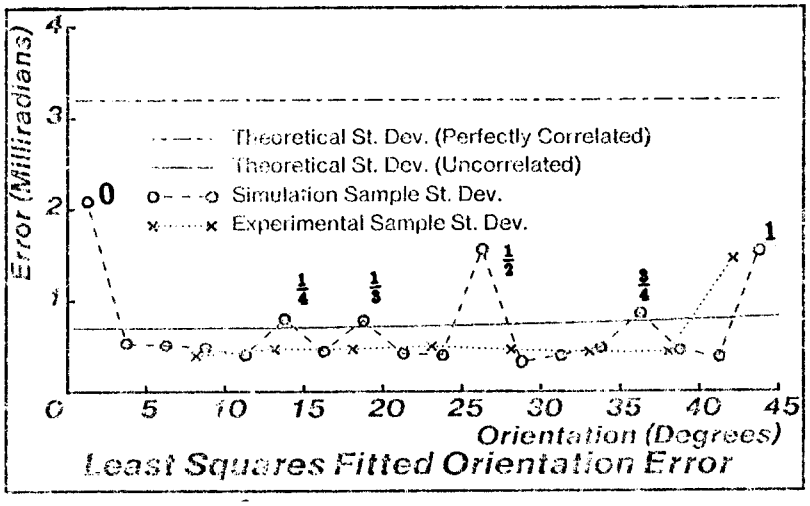

Figure 9: Accuracy of the least squares fitting routine for discretized lines as a function of their orientation. Theoretical, computer simulation and experimental results are shown.

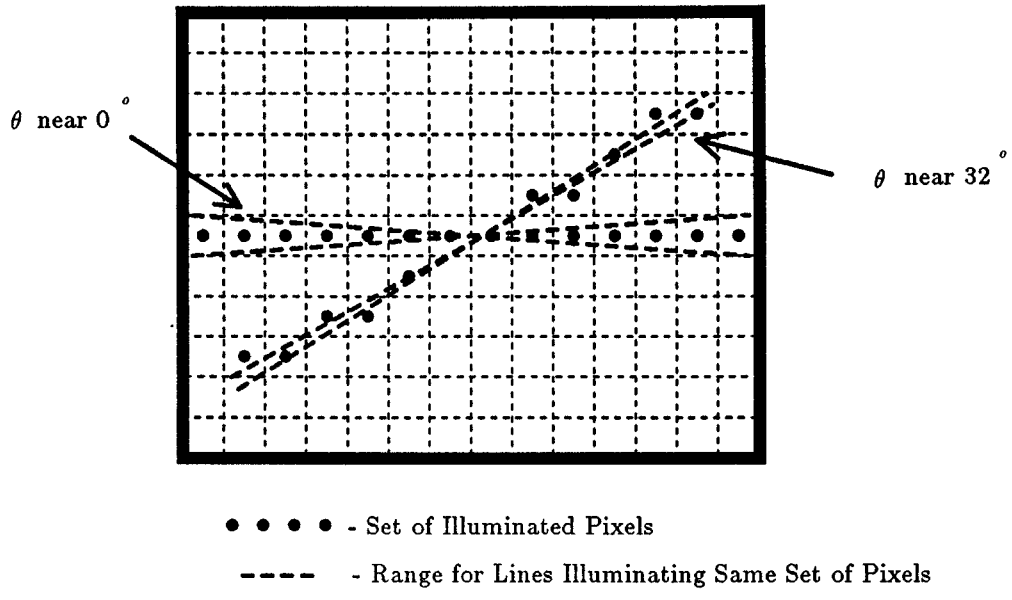

Figure 10: Range of motions of lines before change in state of sensor occurs.

5 Using Redundant Sensed Information

Techniques for combining similar information from a number of sources or multiple measurements from the same source may be used to improve the accuracy of a single measurement [6,7,11,33]. The equivalent of four or more line segments may be generated on a polyhedral feature either by using two or more images with the part or light plane displaced slightly, or by using multiple light planes and a single image. In addition to allowing a more accurate calculation of the location of a part feature, a system of multiple light planes has the advantage of having illumination sources which are not in a single plane; thus, it may be possible to generate longer line segments or have line segments in more desirable locations with respect to the part feature. In fact, some features may be localized with a number of light planes but not with a single light plane.

5.1 Orientation Estimation for Polyhedral Features Without Measurement Covariance Information

This technique does not take the quality of different measurements (covariance) into account. A similar problem is addressed by Faugeras and Hèebert [12,13,14] who find the best fit orientation of an object from a number of sensed normal vectors. We were not able to use their technique since our measurement data is in the form of line segments on the faces of the feature. With each additional line segment, there is an additional equation associated with (10) and we may minimize the sum of the squares of the dot products

$$\min \sum_i (\hat{l}_i \cdot \mathbf{q}\hat{n}_i\mathbf{q}^*)^2. \tag{32}$$

A value for $\mathbf{q}$ which minimizes this quartic expression may be found using a numerical technique.

5.2 Optimal Linear Estimation of Orientation for a Polyhedral Feature

In this technique, the covariance of the measurements are taken into account and a linear estimator is used to estimate the state (position) of the object.

5.2.1 Representation of Rotations

For the subsequent analysis we use an Euler angle description of rotations because the number of variables needed to describe a rotation is equal to the number of degrees of freedom. The Euler angle convention is shown in Figure 11. A coor-

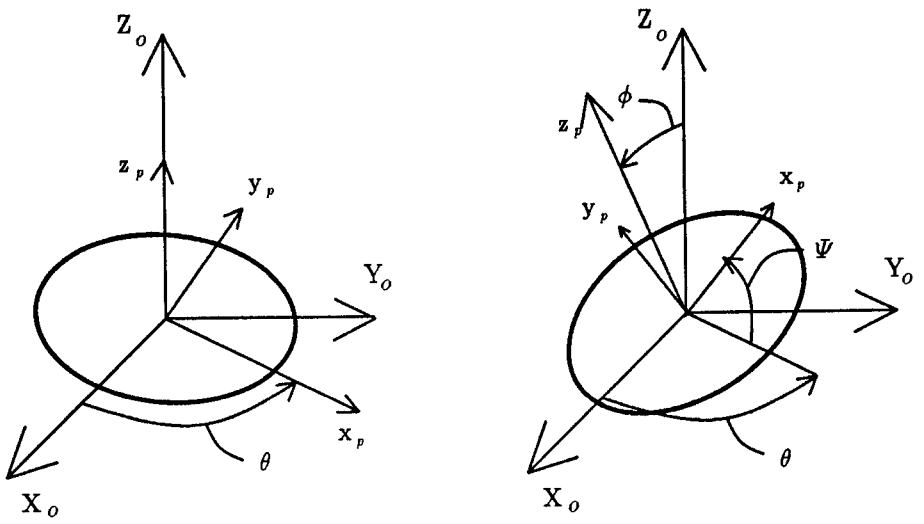

Figure 11: Euler angles used in the least squares estimate for the orientation of a polyhedral feature.

dinate frame located at Euler angles

$$\vec{\alpha} = \begin{Bmatrix} \theta \\ \phi \\ \psi \end{Bmatrix}$$

is first rotated about the base system z axis by angle θ then about its own x axis by angle ϕ, then about its own z axis by angle ψ.

5.2.2 Obtaining an Optimal Linear Estimate from Image Line Slopes

We assume that orientation estimates expressed in Euler angle notation, $\{\vec{\alpha}_i\}$, are available. In general, these may be obtained from three appropriately chosen line segments.

$$\vec{\alpha}_i = \vec{f}_i(S_{i,1}, S_{i,2}, S_{i,3}), \quad i = 1, \ldots, M \tag{33}$$

where $\vec{f}_i$ is a vector function, $S_{i,1}, S_{i,2}$, and $S_{i,3}$ are the slopes of the three line segments from the sensor, and M is the number of different estimates. We wish to combine these estimates to arrive at the most accurate estimate possible, $\hat{\alpha}$, given the expected errors of the measurements.

The functions $\vec{f}_i$ are functions of the calibration variables and part model parameters as well as the slopes of the line segments. For simplicity, only the errors in slopes are considered in the following Kalman filter design. If the magnitude of the unmodeled uncertainties are large enough, imprecise results may be generated.

In general the functions $\vec{f}_i$ in (33) are non-linear and we cannot directly apply linear optimal estimation theory [16]. We can, however, assume that errors in

slope measurements, $\delta S_{i,l}$, are small and linearize (33). Taking the Taylor series expansion and keeping terms of first order or less

$$\vec{\alpha}_i \approx \vec{\bar{\alpha}}_i + \sum_l \frac{\partial \vec{f}_i}{\partial S_{i,l}} \delta S_{i,l} \tag{34}$$

where l takes on the appropriate values for the lines used in the estimates and $\delta S_{i,l}$ is a random variable which is the difference between the actual slope for line l and the measured slope. Neglecting higher order terms, (34) in matrix form is

$$\vec{\alpha}_i = \vec{\bar{\alpha}}_i + \mathbf{K}_{S,i} \delta \vec{S}_i \tag{35}$$

where

$$\mathbf{K}_{S,i} = \left[\frac{\partial \vec{f}_i}{\partial S_{i,1}}, \frac{\partial \vec{f}_i}{\partial S_{i,2}}, \frac{\partial \vec{f}_i}{\partial S_{i,3}} \right] \quad \text{and} \quad \delta \vec{S}_i = \begin{Bmatrix} \delta S_{i,1} \\ \delta S_{i,2} \\ \delta S_{i,3} \end{Bmatrix}. \tag{36}$$

The partial derivatives may be calculated directly if an analytical expression is available for $\vec{f}_i$. If $\vec{f}_i$ involves a numerical technique, the partial derivatives may be approximated by

$$\frac{\partial \vec{f}_i}{\partial S_{i,j}} \approx \frac{\vec{f}_i(S_{i,1}, \ldots, (S_{i,j} + \epsilon), \ldots, S_{i,3})}{\epsilon}$$

where ϵ is a small number whose addition to $S_{i,j}$ will produce a result in the numerical calculation significantly larger than the numerical error.

Rearranging terms, (35) becomes

$$\mathbf{K}_{S,i}^{-1} \vec{\alpha}_i = \mathbf{K}_{S,i}^{-1} \vec{\alpha}_i - \delta \vec{S}_i, \quad i = 1, \ldots, M. \tag{37}$$

All M equations in (37) may be combined into a single equation by adding the rows of each vector term corresponding to the same line segment

$$\vec{z}_S = \mathbf{H}_S \vec{\alpha} + \vec{v}_S \tag{38}$$

where

$$\vec{z}_S = \sum_i \mathbf{K}_{S,i}^{-1} \vec{\bar{\alpha}}_i, \quad \mathbf{H}_S = \sum_i \mathbf{K}_{S,i}^{-1},$$

$$\vec{v}_S = -\sum_i \delta \vec{S}_i.$$

The sums are taken over identical lines only so that (38) has the same number of rows as independent line slopes in the image.

Equation (38) is in the linear optimal estimation equation form [16]; thus, the maximum likelihood estimate for the Euler angles is

$$\hat{\alpha} = (\mathbf{H}_S^T \mathbf{C}_S^{-1} \mathbf{H}_S)^{-1} \mathbf{H}_S^T \mathbf{C}_S^{-1} \vec{z}_S \tag{39}$$

where $\mathbf{C}_S$ is the covariance matrix of the noise vector $\vec{v}_S$. This matrix is diagonal with elements equal to the variances of the slopes of the respective lines. These variances are calculated from (30).

The minimum variance Bayesian estimate of the Euler angles given an *a priori* estimate $\vec{\alpha}-$ and initial covariance matrix $\mathbf{P}^-$ is [16]

$$\hat{\alpha} = \vec{\alpha}^-([\mathbf{P}^-]^{-1} + \mathbf{H}_S^T\mathbf{C}_S^{-1}\mathbf{H}_S)^{-1}\mathbf{H}_S^T\mathbf{C}_S^{-1}(\vec{z}_S - \mathbf{H}_S\vec{\alpha}^-) \tag{40}$$

which is a discrete Kalman filter. This recursive estimator may be applied to position information from fundamentally different sources so long as a measure of the expected accuracy (covariance matrix) of the information is available.

6 Results of Prototype Sensor Accuracy Tests

A prototype light-stripe-part-position sensor mounted in a test bed arrangement is shown in Figure 12. The sensor consists of an MOS-type camera with 320×244 pixels and a laser-cylindrical lens light source. The test bed has three translational stages and three rotational stages.

The measurement accuracy of the test-bed-mounted sensor was studied by measuring the corner feature of a cube, Figure 13. Corner location measurements were compared to the settings on the six stages of the test apparatus. These measurements were relative to an arbitrary reference location. It was not necessary to obtain absolute measurements since relative accuracy is the specification required to determine sensor performance in an assembly environment where all measurements are relative to the robot frame.

The relative accuracy in locating the corner of the cube using information from two light planes was also studied. The maximum likelihood technique developed in Section 5 was used to obtain estimates of the orientation of the cube.

6.1 Test Procedure

The test procedure for determining the accuracy of the sensor entailed locating the cube at a home position then moving one of the six positioning stages (call this the test direction) a small amount. An image of the cube was recorded and the same stage was moved the same amount once again. This was repeated a number of times. The positions of the cube corner from a series of images were compared to the apparatus positions and sample statistics were calculated from differences between stage motion and sensed corner position. The test procedure was repeated for all six stages. The rotational degrees of freedom in stage motion, x_{rot}, ϕ_{rot}, and ψ_{rot} are defined in Figure 13. Measurements were made in the θ, ϕ, and ψ degrees of freedom, which are the Euler angles of the cube. Figure 11 shows the convention

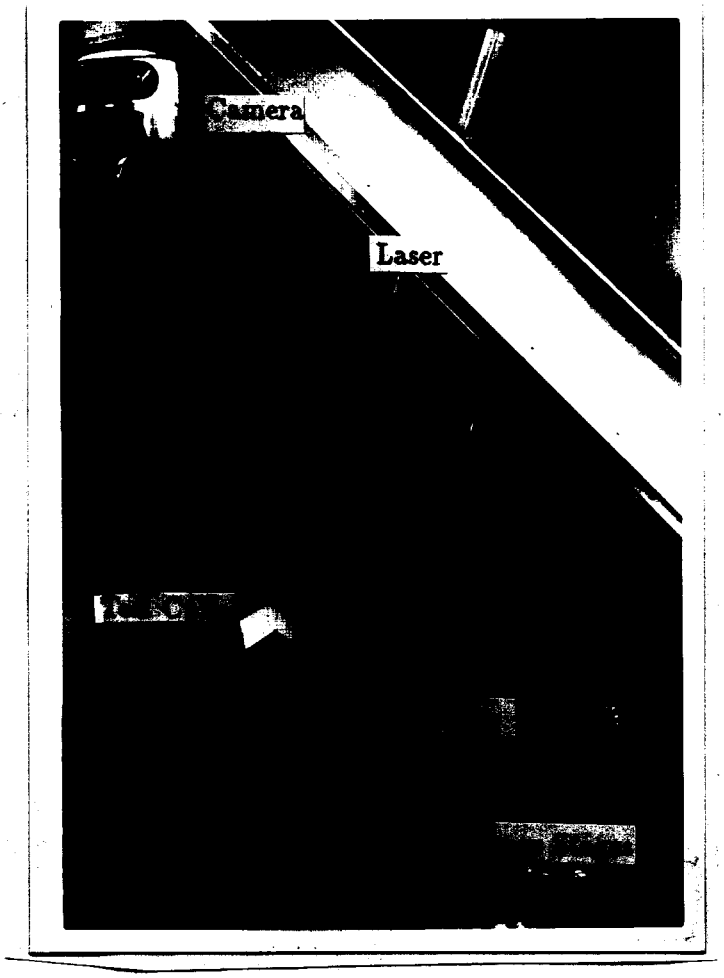

Figure 12: Test bed used for sensor accuracy studies.

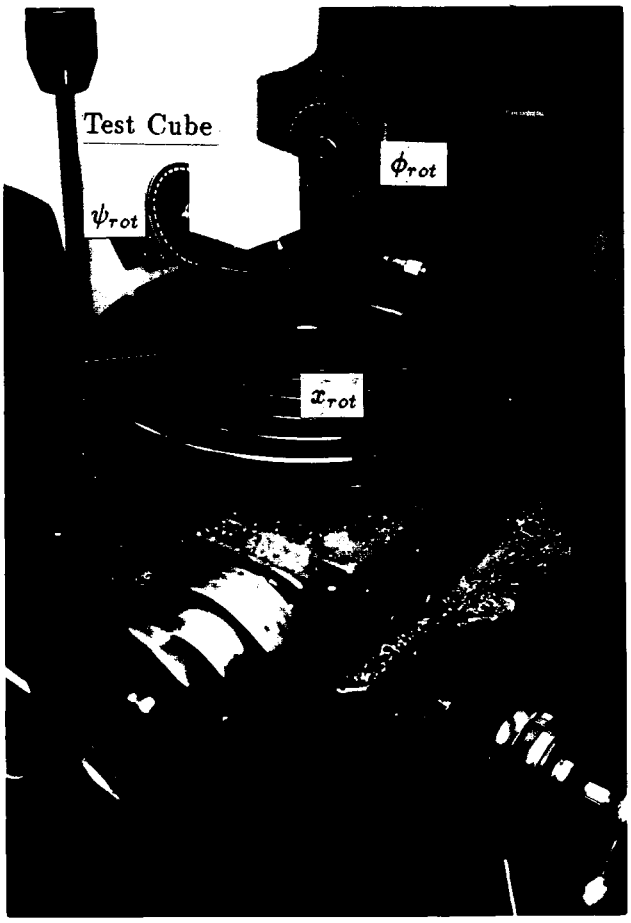

Figure 13: Test cube mounted on rotational stages.

Direction of Motion	Laser Number	X error (inches)	Y error (inches)	Z error (inches)	θ error (degs.)	ϕ error (degs.)	ψ error (degs.)
Trans. X	1	.0030	.0010	.0010	.05	.03	.08
Trans. X	2		.0025	.0015	.13	.04	.11
Trans. Y	1	.0035	.0025	.0015	.12	.09	.14
Trans. Y	2	.0080	.0025	.0025	.12	.05	.13
Trans. Z	1	.0010	.0020	.0025	.11	.07	.13
Trans. Z	2	.0025	.0005	.0015	.15	.06	.14
Rot. ϕ_{rot}	1			.0015		.05	.08
Rot. ϕ_{rot}	2			.0015		.09	.08
Rot. ψ_{rot}	1		.0020		.09		.12
Rot. ψ_{rot}	2		.0020		.14		.08
Rot. x_{rot}	1	.0015					
Rot. x_{rot}	2	.005					

Table 2: Results of the part position sensor accuracy tests. Each number is the sample standard deviation from 21 images. Mean sample standard deviations are: translation – .002 inches (.055 mm), rotation – .095 degrees (.0015 radians).

used. Since the cube was fairly accurately aligned to the axes of the positioner, ϕ_{rot} corresponds closely to ϕ and ψ_{rot} corresponds closely to ψ.

The range of motions for the tests were 0.5 inches (12.7 mm) in each translational degree of freedom and 8.5 degrees (.15 radians) for the ϕ_{rot} rotation and ψ_{rot} rotation and 20 degrees (.35 radians) for the x_{rot} rotation. In general, measurements near the center of the ranges of motion were more accurate than those near the ends. This was because line segments on some cube faces become smaller as the cube was moved from a central position under the laser stripe.

6.2 Single Light Plane Test Results

Table 2 shows the results of the tests for motions of each of the six degrees of freedom. The blank spaces in the table correspond to degrees of freedom which were non-stationary or were not linearly related to the test direction motion. The mean of the sample standard deviations are .002 inches (.05 mm) in translation and 0.095 degrees (0.0015 radians) in rotation. The translational error of .002 inches (.05 mm) is equivalent to about $\frac{1}{4}$ of a camera pixel. Assuming the distribution of errors are Gaussian, 98.8 percent of the measurements (5 standard deviations) will be within an accuracy of .010 inches (.25 mm) and .5 degrees (.007 radians). Each measurement of the position of the cube took about 2.5 seconds. Much of this time was during an image convolution step used to more accurately locate the centers of the line segments [17].

The repeatability of the sensor was extremely high (about .0001 inches or .0025

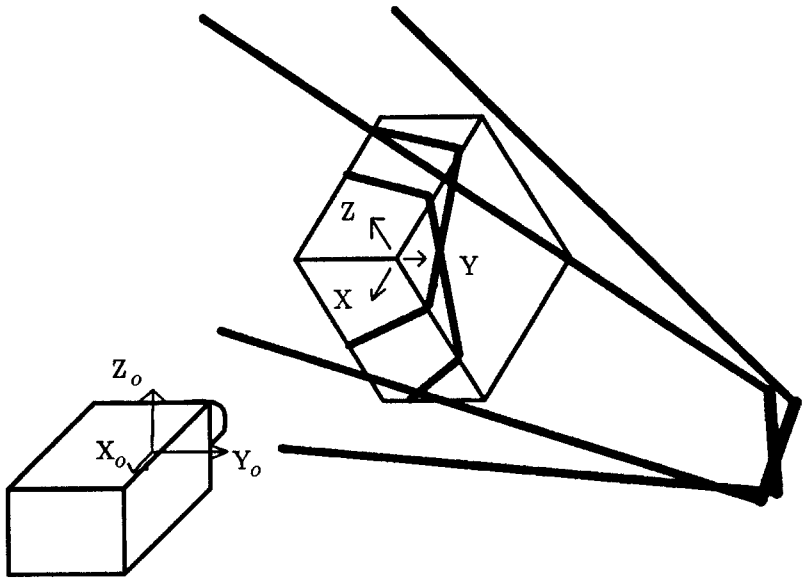

Figure 14: The intersection of two independent light planes with a cube.

mm per standard deviation) when multiple readings were taken without moving the target in between readings. If the target position was perturbed slightly, the readings changed more appreciably (about .001 inches or .025 mm per standard deviation).

In addition to the accuracy tests performed on the testbed, experiments involving assembly of mechanical components using the sensor and a PUMA 600 robot were performed. The sensor-based assembly system was capable of reliably assembling a 36 pin electrical connector, a die cast box, and a 1.75 inch (44.5 mm) square peg-in-hole with a .004 inch (.1 mm) clearance [17,19].

6.3 Multiple Light Plane Test Results

The accuracy in locating the cube's corner using two light stripes was investigated. Six line segments (three from each laser) were generated for each position of the cube, Figure 14. Two independent orientation estimates (Euler angle vectors) were obtained from the line segments and combined using a maximum likelihood technique, (38). Two sets of results were obtained: one with all six estimates being used in a single maximum likelihood calculation, and one with only pairs of corresponding Euler angles being used. When pairs of single Euler angles are used in the estimate, statistical correlations with other Euler angles are ignored. Figure 15 shows the Euler angle estimates for lines from laser number 1, laser number 2, and the maximum likelihood estimate using all six angles. The calculated angles from each of the lasers have different means due to calibration errors. The maximum likelihood estimate does not always fall between the two calculated angles and for

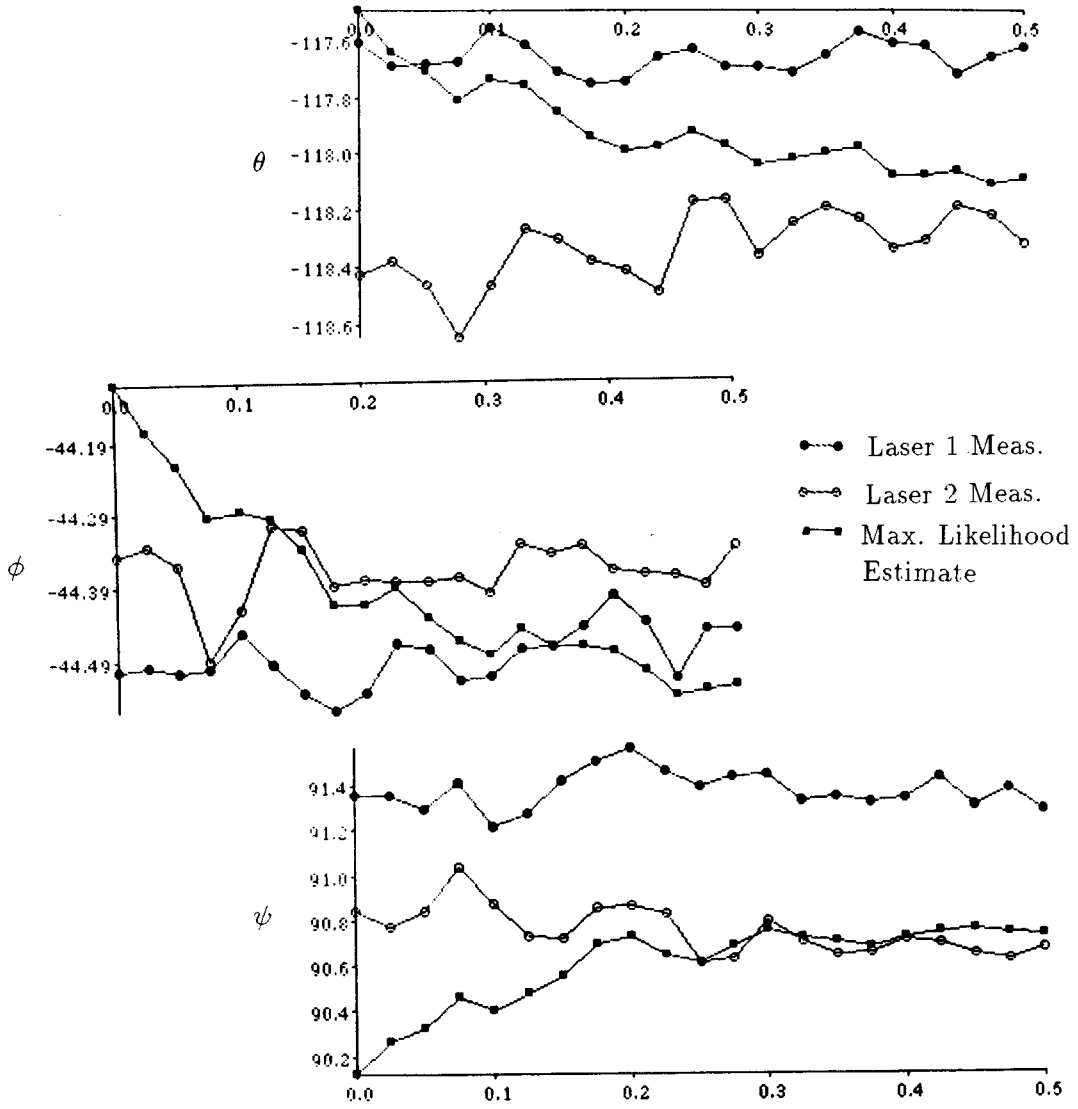

Figure 15: Maximum likelihood estimates of rotation angles of the test cube.

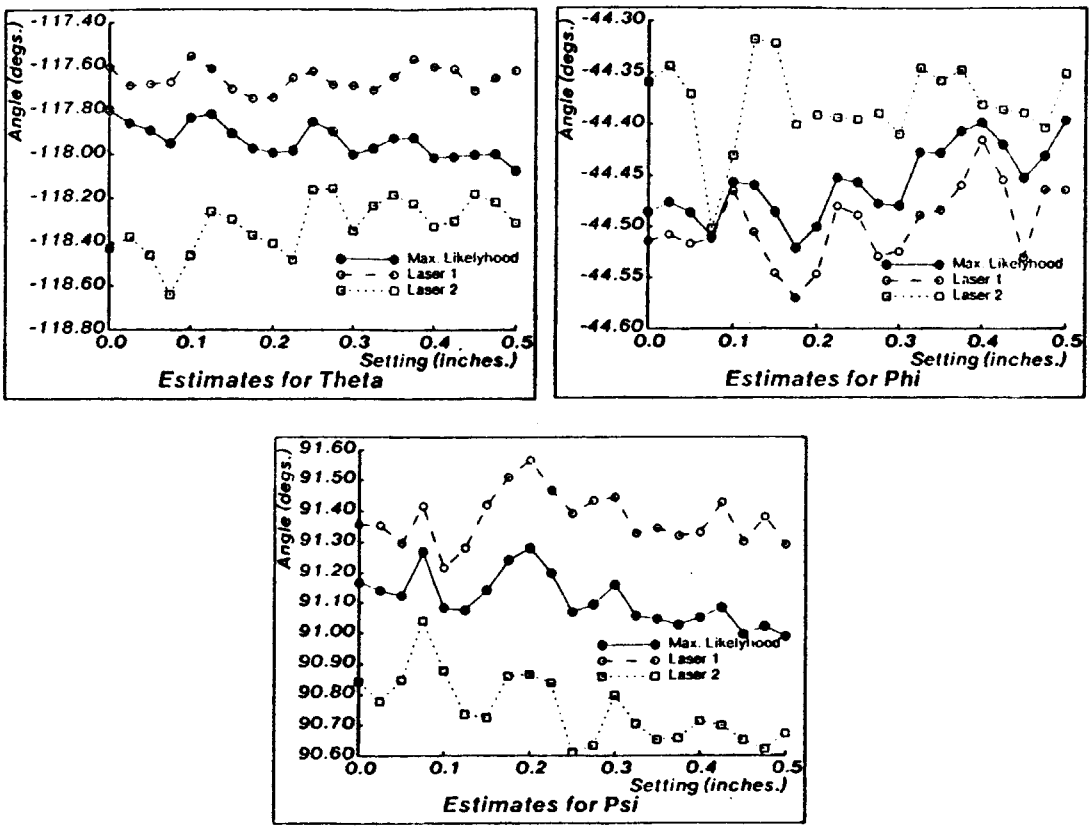

Figure 16: Maximum likelihood estimates of rotation angles of test cube from pairs of angles. Plots are for Euler angles θ, ϕ and ψ.

some angles seems to be an imprecise estimate. This is most likely due to the coupling between the Euler angles and the unmodeled calibration uncertainties. The maximum likelihood estimates from pairs of angles are shown in Figure 16. Here the maximum likelihood estimate is between the two independent laser estimates. The estimate nears one of the single laser estimates when that one is more reliable (longer line segments) than the other. The estimate always uses the combination of the measurements which reduces the overall error. Since calibration errors were not taken into account, the estimate weighs the two calculations equally for equal length line segments. Because the maximum likelihood estimate performs a weighted average of the two estimates, and the two estimates have different means, the sample standard deviation of the maximum likelihood estimate is not always less than the smaller sample standard deviation of the single laser estimates; although, the tests showed that it was usually very close to the lower standard deviation of the two.

7 Summary and Conclusions

A light stripe based vision sensor for locating polyhedral features of parts from a single video frame has been developed. The system locates features to an accuracy

of .002 inches (.05 mm or about $\frac{1}{4}$ of a camera pixel) in translation and about 0.1 degrees (0.0015 radians) in rotation. The measurements take about 2.5 seconds. This may be speeded up to about 1 second if a different hardware image convolver is used.

The calculation for locating general polyhedra requires a numerical computation. If the three planes of the feature are orthogonal, a closed form solution for the feature location may be used. The accuracy of the feature locating technique depends on the lengths of the line segments generated from the intersection of the light plane and the part's planar surfaces. The accuracy of fitting lines to data from quantized images was found as a function of the length, orientation, and position of the segments.

Two techniques for using redundant data from multiple light planes were discussed. One technique may be used to combine measurement data from sources in addition to the light stripe sensor. The covariance of a measurement from the light stripe system is a function of the variance in locating the line segments in the image; thus, the optimal linear estimate weighs those estimates with the longest length segments more than those with shorter length segments.

The sensing system is useful for a number of industrial tasks and was demonstrated to be practical for detecting misalignments between parts prior to their assembly by a manipulator.

Non-polyhedral features generate non-linear curves of intersection and a method of determining the covariance matrix for the parameters of more general curves is required if they are to be incorporated into the optimal estimation technique presented in Section 5. More work is required in sensing non-polyhedral features and analyzing non-linear curves in light stripe images. Bolles and Fischler [9] and Lozano-Pérez, Grimson, and White [25] report difficulty in fitting conic sections to light stripe data. Ellipse fitting, from intersection curves of cylindrical features, gives significantly less accurate results than the line fitting techniques for polyhedral features. We are investigating multiple light plane intersections of cylindrical features which produce additional constraints which could be used in the fitting procedure to give better results (see [25] for a discussion of multiple light plane techniques for fitting cylinders).

References

[1] Acton, F.S., *Analysis of Straight Line Data*, Dover, New York, 1959.

[2] Agapakis, J.E., *Vision-aided Remote Robotic Welding*, Ph.D. Thesis, Dept. of Ocean Engineering, Mass. Inst. of Technology, 1985.

[3] Agin, G.J., Binford T.O., "Computer Description of Curved Surfaces," *Proc. 3rd Int. Joint Conf. Artificial Intell.*, Stanford Univ. Aug 20-23, 1973, pp.629-640.

[4] Beers, Y.B., *Introduction to the Theory of Error*, Addison-Wesley, Reading, Mass., 1957.

[5] Benton, R., Waters, D., *Intelligent Task Automation Interim Technical Reports,* AFWAL/MLTC Wright Patterson AFB, Ohio, Reports 1-7, Oct., 1985.

[6] Bolle, R.M., Cooper, D.B., " On Parallel Bayesian Estimation and Recognition for Large Data Sets with Application to Estimating 3-D Complex-Object Posiiton from Range Data," *Proc. SPIE Conf. Vision for Robots*, Cannes, December, 1985.

[7] Bolle, R.M., Cooper, D.B., " On Optimally Combining Pieces of Information, with Application to Estimating 3-D Complex-Object Position Information," *IEEE Trans. Pattern Anal. Mach. Intell.*, PAMI-8, no.5, September, 1986.

[8] Bolles, R.C., Horaud, P., Hannah, M.J.,, "3DPO: A Three Dimensional Part Orientation System," *Robotics Research: The First Symposium* (Brady, M. Paul, R. eds.), MIT Press, Cambridge, Mass. 1984.

[9] Bolles, R.C., Fischler, M.A., "A RANSAC-Based Approach to Model Fitting and Its Application to Finding Cylinders in Range Data," *Proc. 7^{th} Int. Joint Conf. Artificial Intell.*, 1981, pp.637-643.

[10] Drake, A.W., *Fundamentals of Applied Probability Theory*, McGraw-Hill, New York, 1967.

[11] Durrant-Whyte, H.F., "Consistant Integration and Propagation of Disparate Sensor Observations," *IEEE Inter. Conf. on Robotics and Automation*, San Francisco, 1986, pp.1464-1469.

[12] Faugeras, O.D., Hébert, M., Pauchon, E., Ponce, J., "Object Representation, Identification, and Positioning from Range Data," *Robotics Research: The First Symposium* (Brady, M. Paul, R. eds.), MIT Press, Cambridge, Mass. 1984.

[13] Faugeras, O.D., "New Steps Toward a Flexible 3-D Vision System for Robotics," *2^{nd} Int. Symp. on Robotics Research*, Kyoto, Japan, 1984.

[14] Faugeras, O.D., Hébert, M., "The Representation, Recognition and Locating of 3-D Objects," *Int. J. Robotics Res.*, v.5, no.3, 1986, pp.27-52.

[15] Faux, I.D., Pratt, M.J., *Computational Geometry for Design and Manufacture*, Ellis Horwood Ltd., Chinchester, England, 1979.

[16] Gelb, A. (ed.), *Applied Optimal Estimation*, MIT Press, Cambridge, Mass., 1974.

[17] Gordon, S.J., "Automated Assembly Using Feature Localization," Ph.D. Thesis, Dept. of Mechanical Engineering, Mass. Inst. of Technology, Oct. 1986; also, Technical Report no.932, M.I.T. Artificial Intelligence Laboratory, Cambridge, Mass., 1986.

[18] Gordon, S.J., Seering, W.P., "Accuracy Issues in Measuring Quantized Images of Straight-Line Features," *IEEE Inter. Conf. on Robotics and Automation*, San Francisco, 1986, pp.931-936.

[19] Gordon, S.J., Seering, W.P., "Position-Sensor-Driven Assembly," *IEEE Inter. Conf. on Robotics and Automation*, Raleigh N. Carolina, 1987, pp.801-806.

[20] Grimson, W.E.L., "Disambiguating Sensory Interpretations Using Minimal Sets of Sensory Data," *IEEE Inter. Conf. on Robotics and Automation*, San Francisco, 1986, pp.286-292.

[21] Grimson, W.E.L., Lozano-Pérez, T., "Model-Based Recognition and Localization from Sparse Range or Tactile Data," *Int. J. Robotics Res.*, v.3, no.3, 1984, pp.3-35.

[22] Hill, J. "Dimensional Measurements from Quantized Images," *Machine Intelligence Research Applied to Industrial Automation (Tenth Report)*, SRI Int., Menlo Park, Calif., 1980, pp.75-106.

[23] Horn, B.K.P., *Robot Vision*, MIT Press, Cambridge, Mass. 1986.

[24] Jarvis, R.A., "A Perspective on Range Finding Techniques for Computer Vision," *IEEE Trans. Pattern Anal. Mach. Intell.*, PAMI-5, no.2, March, 1983.

[25] Lozano-Pérez, T., Grimson, W.E.L., White, Steven J., "Finding Cylinders in Range Data," *IEEE Inter. Conf. on Robotics and Automation*, Raleigh N. Carolina, 1987, pp.202-207.

[26] Nitzan, D., et. al., *Machine Intelligence Research Applied to Industrial Automation,* Technical Report no.12, SRI Project 2996, SRI Int., Menlo Park, Calif., 1983.

[27] Oppenheim, A.V., Shafer, R.W., *Digital Signal Processing*, Prentice-Hall, Englewood Cliffs, New Jersey, 1975.

[28] Pervin, E., Webb, J.A., "Quaternions in Computer Vision and Robotics," Department of Computer Science, Carnegie-Mellon Univ., CMU-CS-82-150, 1982.

[29] Rutkowski, W.S., Benton, R., Kent, E.W., "Model-Driven Determination of Object Pose for a Visually Servoed Robot," *IEEE Inter. Conf. on Robotics and Automation*, Raleigh N. Carolina, 1987, pp.1419-1428.

[30] Popplestone, R.J., Brown, C.M., Ambler, A.P., Crawford, G.F., "Forming Models of Plane and Cylinder Faceted Bodies from Light Stripes," *Proc. 5^{th} Int. Joint Conf. Artificial Intell.*, 1975, pp.664-668.

[31] Salamin E., "Applicaiton of Quaternions to Computation with Rotations," unpublished, internal memo, Stanford Artificial Intelligence Lab, 1979.

[32] Salisbury, J.K., Jr., *Kinematic and Force Analysis of Articulated Hands*, PhD. Thesis, Dept. of Mechanical Engineering, Stanford University, May, 1982; also Stanford Department of Computer Science Report No.STAN-CS-82-921; also in Mason, M.T., Salisbury, J.K., Jr., *Robot Hands and the Mechanics of Manipulation*, MIT Press, Cambridge, Mass, 1986.

[33] Shekhar S., Khatib, O., Shimojo M., "Sensor Fusion and Object Localization," *IEEE Inter. Conf. on Robotics and Automation*, San Francisco, 1986, pp.1623-1628.

[34] Shirai, Y., Suwa, M., "Recognition of Polyhedrons with a Range Finder," *Proc. 2nd Int. Joint Conf. Artificial Intell.*, 1971, pp.80-87.

[35] Smith, F.G., Thomson, J.H., *Optics*, John Wiley and Sons, Chinchester, 1971.

CS-TR Scanning Project
Document Control Form

Date : 4/27/95

Report # AIM-1032

Each of the following should be identified by a checkmark:
Originating Department:

☒ Artificial Intellegence Laboratory (AI)
☐ Laboratory for Computer Science (LCS)

Document Type:

☐ Technical Report (TR) ☒ Technical Memo (TM)
☐ Other:_____

Document Information

Number of pages: 32 (38-IMAGES)
Not to include DOD forms, printer instructions, etc... original pages only.

Originals are:
☒ Single-sided or
☐ Double-sided

Intended to be printed as :
☐ Single-sided or
☒ Double-sided

Print type:
☐ Typewriter ☐ Offset Press ☒ Laser Print
☐ InkJet Printer ☐ Unknown ☐ Other:_____

Check each if included with document:

☒ DOD Form (2) ☐ Funding Agent Form ☐ Cover Page
☐ Spine ☐ Printers Notes ☐ Photo negatives
☐ Other: _____

Page Data:

Blank Pages (by page number):_____

Photographs/Tonal Material (by page number): 23, 24

Other (note description/page number):

Description :	Page Number:
(A) IMAGE MAG (1-32) UNNUMBERED PAGES	1-32
(33-35) SCANCONTROL, DOD(2)	
(36-38) TARGETS (3)	
(B) CUT+PASTE FIGS ON IMAGE #	3-7, 10, 12-14, 17-18, 20, 23, 24, 26-28

Scanning Agent Signoff:
Date Received: 4/27/95 Date Scanned: 5/3/95 Date Returned: 5/4/95

Scanning Agent Signature: Michael W. Cook

UNCLASSIFIED

SECURITY CLASSIFICATION OF THIS PAGE (When Data Entered) CDR 3-28-89

REPORT DOCUMENTATION PAGE

READ INSTRUCTIONS BEFORE COMPLETING FORM

1. REPORT NUMBER: AIM 1032	2. GOVT ACCESSION NO.: A203580
3. RECIPIENT'S CATALOG NUMBER:	
4. TITLE (and Subtitle): Real-Time Position Sensing	5. TYPE OF REPORT & PERIOD COVERED: memorandum
	6. PERFORMING ORG. REPORT NUMBER:
7. AUTHOR(s): Steven J. Gordon	8. CONTRACT OR GRANT NUMBER(s): N00014-85-K-0124
9. PERFORMING ORGANIZATION NAME AND ADDRESS: Artificial Intelligence Laboratory 545 Technology Square Cambridge, MA 02139	10. PROGRAM ELEMENT, PROJECT, TASK AREA & WORK UNIT NUMBERS:
11. CONTROLLING OFFICE NAME AND ADDRESS: Advanced Research Projects Agency 1400 Wilson Blvd. Arlington, VA 22209	12. REPORT DATE: May 1988 13. NUMBER OF PAGES: 32
14. MONITORING AGENCY NAME & ADDRESS (if different from Controlling Office): Office of Naval Research Information Systems Arlington, VA 22217	15. SECURITY CLASS. (of this report): UNCLASSIFIED 15a. DECLASSIFICATION/DOWNGRADING SCHEDULE:

16. DISTRIBUTION STATEMENT (of this Report)

Distribution is unlimited

17. DISTRIBUTION STATEMENT (of the abstract entered in Block 20, if different from Report)

Unlimited

18. SUPPLEMENTARY NOTES

None

19. KEY WORDS (Continue on reverse side if necessary and identify by block number)

real-time vision	light stripe sensor
sensor based assembly	quantization errors
vision for manipulation	sensor data fusion

20. ABSTRACT (Continue on reverse side if necessary and identify by block number)

A light stripe vision system is used to measure the location of polyhedral features of parts from a single frame of video camera output. The geometric conditions which assure location of the feature when the light plane intersects three of the feature's faces are given. Issues such as accuracy in locating the line segments of intersection in the image and combining redundant information from multiple measurements and multiple sources are addressed. In 2.5 seconds, a prototype sensor was capable of locating a two inch cube to an accuracy (one standard deviation) of .002 inches (.055 mm) in translation

DD FORM 1 JAN 73 1473 EDITION OF 1 NOV 65 IS OBSOLETE
S/N 0102-014-6601

UNCLASSIFIED

SECURITY CLASSIFICATION OF THIS PAGE (When Data Entered)

UNCLASSIFIED

SECURITY CLASSIFICATION OF THIS PAGE (When Data Entered)

REPORT DOCUMENTATION PAGE	READ INSTRUCTIONS BEFORE COMPLETING FORM
1. REPORT NUMBER: AIM 1032	2. GOVT ACCESSION NO. A190358
4. TITLE (and Subtitle): Real-Time Position Sensing	3. RECIPIENT'S CATALOG NUMBER
7. AUTHOR(s): Steven J. Gordon	5. TYPE OF REPORT & PERIOD COVERED: Memorandum
9. PERFORMING ORGANIZATION NAME AND ADDRESS: Artificial Intelligence Laboratory, 545 Technology Square, Cambridge, MA 02139	6. PERFORMING ORG. REPORT NUMBER
11. CONTROLLING OFFICE NAME AND ADDRESS: Advanced Research Projects Agency, 1400 Wilson Blvd., Arlington, VA 22209	8. CONTRACT OR GRANT NUMBER(s): N00014-85-K-0124
12. REPORT DATE: May 1988	10. PROGRAM ELEMENT, PROJECT, TASK AREA & WORK UNIT NUMBERS
13. NUMBER OF PAGES: 32	
14. MONITORING AGENCY NAME & ADDRESS (if different from Controlling Office): Office of Naval Research, Information Systems, Arlington, VA 22217	15. SECURITY CLASS. (of this report): UNCLASSIFIED
	15a. DECLASSIFICATION/DOWNGRADING SCHEDULE

16. DISTRIBUTION STATEMENT (of this Report)

Distribution is unlimited

17. DISTRIBUTION STATEMENT (of the abstract entered in Block 20, if different from Report)

Unlimited

18. SUPPLEMENTARY NOTES

None

19. KEY WORDS (Continue on reverse side if necessary and identify by block number)

real-time vision
sensor based assembly
vision for manipulation
light stripe sensor
quantization errors
sensor data fusion

20. ABSTRACT (Continue on reverse side if necessary and identify by block number)

A light stripe vision system is used to measure the location of polyhedral features of parts from a single frame of video camera output. The geometric conditions which assure location of the feature when the light plane intersects three of the feature's faces are given. Issues such as accuracy in locating the line segments of intersection in the image and combining redundant information from multiple measurements and multiple sources are addressed. In 2.5 seconds, a prototype sensor was capable of locating a two inch cube to an accuracy (one standard deviation) of .002 inches (.055 mm) in translation

DD FORM 1473 (1 JAN 73) EDITION OF 1 NOV 65 IS OBSOLETE S/N 0102-014-6601

UNCLASSIFIED

SECURITY CLASSIFICATION OF THIS PAGE (When Data Entered)

Scanning Agent Identification Target

Scanning of this document was supported in part by the **Corporation for National Research Initiatives,** using funds from the **Advanced Research Projects Agency** of the **United states Government** under Grant: **MDA972-92-J1029.**

The scanning agent for this project was the **Document Services** department of the **M.I.T Libraries.** Technical support for this project was also provided by the **M.I.T. Laboratory for Computer Sciences.**